View Online

Three-dimensional surface microfluidics enabled by spatiotemporal control of elastic fluidic interface†

Lingfei Hong[ab] and Tingrui Pan*[a]

Received 6th July 2010, Accepted 21st September 2010
DOI: 10.1039/c0lc00173b

Downloaded by Library of Chinese Academy of Sciences on 26 November 2010
Published on 09 November 2010 on http://pubs.rsc.org | doi:10.1039/C0LC00173B

As an emerging alternative to the conventional counterpart, surface microfluidics incorporates both intrinsic resistive solid-liquid and elastic frictionless gas-liquid interfaces, leading to unique flow-pressure characteristics. Furthermore, the open-surface microfluidic platforms can be fabricated on a monolithic substrate with high wettability contrast by the previously reported one-step lithographic process of a photosensitive superhydrophobic nanocomposite material, which permits flexible fluidic operations and direct surface modifications. In the paper, we first present three-dimensional microfluidic manipulations utilizing the unconventional gas-liquid interfaces of surface microfluidics, outlined by the micropatterned wetting boundaries (also known as the triple lines). In contrast to the primary linear (resistive) nature of the conventional closed-channel microfluidics, the distinct elastic interface of surface microfluidics enables remarkable three-dimensional (deformable) and time-dependent (capacitive) operations of the flow. Specifically, spatiotemporal dependence of microflow patterns on the planar fluidic surfaces has been theoretically analyzed and experimentally characterized. Utilizing the unconventional interface-enabled flow-pressure relationship, novel surface fluidic operations, including microflow regulation and flow-controlled switching, have been demonstrated and fully investigated. Furthermore, three-dimensional surface microfluidic networks together with analog-to-digital stereo-flow activations have been established, in which miniature capillary bridges form fluidic connections between two independent surface microfluidic circuits.

Introduction

Microfluidics has been widely employed in chemical and biological analyses over the past decades.[1–3] Constructed by a large variety of microfabrication techniques, microfluidics offers highly desired features, including minute amounts of reagents, accelerated reaction rates, process integrateability and multiplexability, in comparison with the conventional fluidic systems.[4–9] However, majority of microfluidic devices require spatial confinement of flow in a closed-channel configuration, which usually involves complex multilayer fabrication and packaging of the fluidic conduits. Moreover, any gas-liquid interface (*e.g.*, bubble trapping) encountered in an enclosed microchannel could lead to unexpected impediment to fluidic operations, which becomes even more problematic with further device miniaturization.

Surface microfluidics, an emerging alternative to the conventional microfluidics, addresses the aforementioned obstacles, and has received increasing attention from microfluidic community.[10–12] Enabled by the latest advances in interfacial chemistry as well as microfabrication techniques, planar microfluidic pathways can be lithographically defined by the high contrast of interfacial energies, which consequently determines the surface wettability.[13–18] The boundaries presented between wetted and unwetted areas, also known as the triple lines (of gas-liquid-solid interphases), serve as virtual borders for fluid flow. The surface wettability-guided microflow is first demonstrated in a closed-channel configuration, where two immiscible liquids flow along the wettability boundary instead of following solid geometric confinement.[19] Later investigations primarily employ double planar surface configuration to direct surface microflow, referred to as the surface directed microchannels, of which either identical wetting patterns are established or wetting patterns on one-side and hydrophobicity on the other.[17,19–28] A number of micropatterning techniques, including photolithography, inkjet printing, lift-off, and plasma etching, have been applied to define surface wettability contrast (*i.e.*, hydrophilic patterns on hydrophobic substrates or vice versa) as summarized in Table 1.

Besides the aforementioned surface patterning methods, our group has previously developed a one-step photo-patterning technique to fabricate nanocomposite structures with ultrahigh wettability contrast on any planar surface.[11,12] In the paper, using the photosensitive hydrophobic nanocomposite formula (with water contact angle > 165°), we have demonstrated surface microfluidic operations on a single planar substrate, where the flow is confined by the interphase triple lines along the superhydrophobic microstructures on the hydrophilic surface. The packaging-free open-surface monolithic platform, incorporating both inflexible resistive solid-liquid and elastic frictionless gas-liquid interfaces, permits direct environmental access, flexible fluidic operations, and easy surface modification, as well as

[a]*Micro-Nano Innovations (MiNI) Laboratory, Department of Biomedical Engineering, University of California, Davis, USA. E-mail: tingrui@ucdavis.edu*
[b]*School of Instrumentation Science and Optoelectronics Engineering, Beihang University, Beijing, China*

† Electronic supplementary information (ESI) available: The equivalent circuit model for the two-stage analog-to-digital flow activation. Movies of the flow regulation, flow-controlled switching, and analog-to-digital stereo-flow activation. See DOI: 10.1039/c0lc00173b

View Online

Table 1 Summary of microfabrication and packaging techniques for surface microfluidics

Authors	Microfabrication Methods	Packaging
Zhao, et al.[13,19] Lee, et al.[27] Besson, et al.[28]	Photopattern synthesized hydrophobic SAMs on cover glasses	Surface microfluidic circuits configured in between two substrates either with identical wetting patterns on both sides or patterned on one side and hydrophobic on the other
Lam, et al.[26] Watanabe, [17,22] Swickrath, et al.[4,23]	Print hydrophilic ink on pre-treated hydrophobic surfaces	
West, et al. [16] Yang, et al.[30]	Use plasma treatment to remove part of pre-deposited hydrophobic molecules	
Bouaidat, et al.[15]	Lift off hydrophobic features on hydrophilic surface	
Gau, et al.[20]	Deposit hydrophilic molecules onto hydrophobic substrate	Surface microfluidics performed on a single-side patterned substrate with high-wettability contrast
Juncker, et al.[21]	Contact printing of hydrophobic molecules to hydrophilic substrate using PDMS stamp	
Hong and Pan[11,12]	Use single-step photolithography to create superhydrophobic micropatterns on hydrophilic surfaces	

Downloaded by Library of Chinese Academy of Sciences on 26 November 2010
Published on 09 November 2010 on http://pubs.rsc.org | doi:10.1039/C0LC00173B

eliminates the interfacial cavitation problems (*e.g.*, gas bubble generation).[29] Furthermore, analytical and experimental investigations have been presented to spatiotemporally manipulate the flexible gas-liquid interface in surface microfluidics, which introduces geometrical expansion (deformability) and thereby fluidic compliance (capacitance) to the laminar microflow, analogous to stray capacitance in electronics. As a result, the pressure gradient not only propels the fluid but controls the three-dimensional profile of the flow. Moreover, the interfacial compliance/capacitance adds temporal dependence to the surface flow. Based on the unique spatiotemporal flow-pressure characteristics, new microfluidic operations, including microflow regulation and flow-controlled switching, have been demonstrated and fully investigated. Furthermore, stereo surface microfluidic networks together with analog-to-digital flow activations have been established, in which capillary bridges form fluidic connections between two independent surface microfluidic circuits.

Theoretical analysis

Considering the substantial differences in fluid mechanics between the surface and closed-channel microfluidics, in depth microfluidic analysis is of essential importance to the emerging direction. Specifically, the distinct out-of-plane elastic gas-liquid interface could potentially enable spatiotemporal manipulation of the flow due to the presence of fluidic compliance/capacitance and interfacial elasticity, similar to the operation of the capillarity-enabled stop valves.[30–34] To understand the nonlinear flow-pressure characteristics in surface fluidics, an equivalent lumped-element model has been established. Similar to the transmission line theory in radiofrequency circuitry, the distributed-parameter network is used to describe the resistive and capacitive nature of the fluidics in an infinitesimal length.[35] Whereas, the resistance (R) and capacitance (C) in surface microfluidics are flow- or pressure-dependent (that is, R and C vary with the change of flow rate or pressure). For instance, in a straight surface microchannel, flow passing through the resistive solid-liquid boundary generates a continuous pressure gradient. Meanwhile, deformed by the induced pressure drop, the elastic gas-liquid interface accommodates fluidic accumulation and alters the cross-sectional area. As a consequence, the flow resistance is adaptively modified by the influx rate. Fig. 1-a represents the lumped-element model describing flow characteristics of a general surface fluidic network using the distributed parameters.

Despite the complex nature of surface microflow, the assumption of extremely low Reynolds number (Re) can be applied to simplify the flow-pressure (Q-P) relationship. In such cases, the pressure difference across the flexible gas-liquid interface calculated from Laplace equation serves as the primary driven forces to the flow. Two basic circuit elements, straight channels and circular reservoirs, are therefore introduced in place of fluidic resistance and capacitance. Under a flow with low Re (< 10), straight microchannels can be approximated as primarily resistive elements as long as the deformation of the gas-liquid interface is insignificant. According to our previous study, it is particularly valid when compared to the lateral expansion of the circular reservoirs under low-Re flows.[11] On the other hand, the circular reservoirs present substantially less resistance to the flow, but experience mainly interfacial deformation even with a slight pressure elevation predicted by Laplace equation, which resembles capacitive characteristics in fluidic circuitry. Given geometrical confinements, the resistance of microchannels[36] and the capacitance of micro-reservoirs can be calculated from the following equations, respectively:

 This journal is © The Royal Society of Chemistry 2010

View Online

Downloaded by Library of Chinese Academy of Sciences on 26 November 2010
Published on 09 November 2010 on http://pubs.rsc.org | doi:10.1039/C0LC00173B

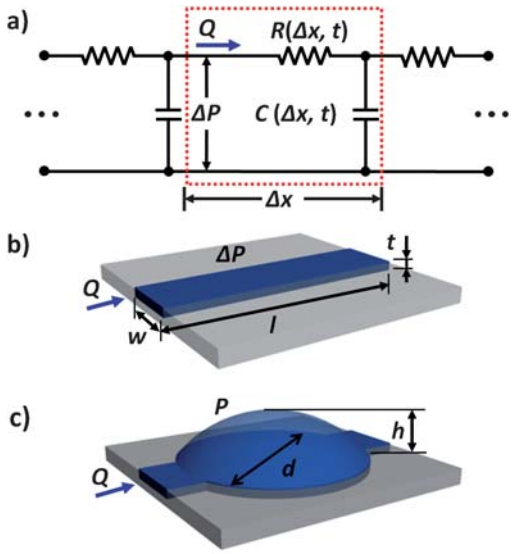

Fig. 1 (a) Distributed lumped-element model of surface microfluidics describing the combined resistive and capacitive nature along with two simplified basic components: (b) the resistive straight microchannel with unaltered gas-liquid boundary, and (c) the capacitive circular micro-reservoir with deformable interface.

$$R = \frac{dP}{dQ} = \frac{3\mu l}{wt^3} \qquad \text{(Eq 1)}$$

$$C = \frac{dV}{dP} = \frac{\pi\left(4h^2 + d^2\right)^3}{128\gamma\left(d^2 - 4h^2\right)} \qquad \text{(Eq 2)}$$

where μ is the dynamic viscosity of the fluid, γ is the liquid surface tension, l, w, and t are the length, width and height of the microchannel, respectively, whereas, d indicates the diameter of the reservoir and the fluidic height is shown as h (the detailed derivation can be found in ESI). Fig. 1-b and 1-c illustrate the corresponding geometrical parameters in the fluidic circuit elements. Incorporating the resistive and capacitive elements with the interfacial deformability into the fluidic circuitry, new spatiotemporal operations of surface flow can be developed.

Experimental methods

Planar surface fluidic structures are microfabricated by a single-step photo-patterning technique reported previously.[11] In this process, a photosensitive hydrophobic nanocomposite formula is applied to create nanostructures with ultrahigh wettability contrast to the hydrophilic surfaces, in which polytetrafluoroethylene (PTFE) nanoparticle filler (Microdispers-200, Polyscience, Inc.) with extremely low chemical energy and nanotopology is embedded in a photopatternable SU-8 polymer matrix (SU-8 2050, MicroChem Corp.). The surface micromachining begins with spin-coating a 30μm-thick layer of SU-8 photoresist onto an acid-cleaned glass substrate. Subsequent to soft bake at 95 °C and ultraviolet exposure at 150 mJ/cm^2 through a photomask, the superhydrophobic nanocomposite suspension (of PTFE/SU-8 mixture) in an ethanol solution, is uniformly spray-coated onto the exposed SU-8 layer with 2μm in thickness. Post-exposure bake is conducted at 95 °C followed by the development step of the unexposed area in SU-8 developer. Subsequently, the micropatterned surface is rinsed with isopropyl alcohol (IPA) and deionized (DI) water, and finally air-dried.

The three-dimensional microfluidic networks are formed by placing two microfabricated planar fluidic structures face-to-face with spacers, and surface flow between two chips is connected through miniature capillary bridges formed between the capacitive elements (reservoirs). The spacers are made of cured polydimethylsiloxane (PDMS) blocks (10 : 1 ratio of the precursor to curing agent, Dow Corning) with different heights (from 200 μm to 600 μm). Both DI water and diluted aqueous-based color dyes (Waterman, France) are used to evaluate the fluidic performance. A programmable syringe pump (KD Scientific) directly injects the fluid into the inlet reservoir or channel through a 30 gauge needle (PrecisionGlide). The needle is pointed towards the hydrophilic injection site with one hundred micrometer separation, where capillary bridge between the channel and the needle will form during the injection process to keep real-time flow rate variation. The pressure difference across the interface is assessed by measuring the elastic curvature through a high-speed digital microscope. The overall flow rate is assessed at a steady-state condition.

Results and discussion

Incorporating both capacitive and resistive elements into microfluidic design, new surface fluidic functionality (*e.g.*, nonlinear pressure-flow responses) can be implemented. Furthermore, the frictionless yet elastic gas-liquid interface enables three-dimensional manipulations of the flow (*e.g.*, forming capillary bridges between two parallel wettable surfaces). Combining the unique out-of-plane spatiotemporal dependence of the surface microfluidics, three-dimensional surface microfluidic operations, including microflow regulation, flow controlled switching, and analog-to-digital stereo-flow activations, will be demonstrated and characterized in the following section.

Microflow regulation

Microflow regulators have been used in management of specific flow characteristics (*e.g.*, flow limiting or pressure damping), and usually involve active controlling units with particular structural design, which requires complicated micromachining and device packaging.[37,38] Here we present a simple flow-limiting mechanism enabled by the direct correlation between the interfacial geometry and hydraulic pressure of surface flow. The surface fluidic regulator only comprises a circular reservoir as the functional element connecting to resistive fluidic channels, as shown in Fig. 2-a. When flow passes through the reservoir, a pressure head established inside is determined by the radius of curvature of liquid accumulation. A smaller radius of curvature leads to a higher hydraulic pressure, according to Laplace equation,[7] whereas, the maximal pressure head is achieved as the gas-liquid interface reaches a hemi-spherical shape (*i.e.*, the radius of curvature equal to that of the reservoir), as indicated in the case 2 in Fig. 2-a. Further increasing (case 1) or decreasing (case 3) the

View Online

Downloaded by Library of Chinese Academy of Sciences on 26 November 2010
Published on 09 November 2010 on http://pubs.rsc.org | doi:10.1039/C0LC00173B

liquid volume in the reservoir will lead to rise in the radius of curvature and thus, reduced Laplace pressure and outflow rate. In brief, the reservoir geometry sets the maximal pressure head and the through-flow limits.

To experimentally verify the microflow regulation principle, the flow-limiting devices with various reservoir sizes (from 500μm to 3mm in diameter) are fabricated with the connecting channels of constant dimensions (of 200μm in width, 40μ in depth, and 2cm in length). Fig. 2-b shows the experimental results of the maximal flow rates passing through the flow-regulating reservoirs plotted with the theoretical simulations. Under lower flow rates, the outflow (Q_{out}) keeps the same pace as the influx (Q_{in}) in a steady state, where the accumulated fluid in the reservoir forms a sub-hemispherical shape (in case 1). When the flow reaches the maximal flow rate (Q_{max}), Laplace pressure achieves its maximum, leading to a hemi-spherical shape (in case 2). Further increase of the flow rate leads to fluidic instability with positive feedback. In this scenario, the outflow rate cannot catch up with the influx, the volume of accumulated liquid keeps rising, and so does the radius of curvature. As a result, the dropping pressure head inside the reservoir further reduces the outflow and causes unstable liquid buildup (in case 3). Therefore, the maximal outflow is solely regulated by the geometrical confinement of the circular reservoir (see Movie 1 in ESI). As can be seen, the measurements are well agreed with the simulations in the larger reservoirs (d > 1,000μm); however, a rising divergence from theoretical predictions has also been observed with the reduced size of the reservoirs (d < 1,000μm). This could be attributed to the additional fluidic conductance casued by the deformed interface extended to the connecting channels. Inserts in Fig. 2-b illustrates the interfacial deformation in a circular reservoir of 1,000μm in diameter with the disturbed liquid profile (*e.g.*, formation of meniscus) in the microchannels.

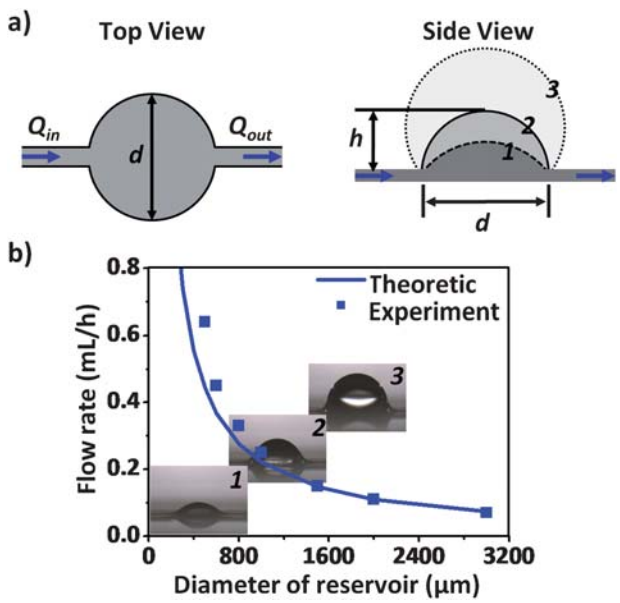

Fig. 2 (a) Illustration of microflow regulator design with three states: stable (case 1), maximal/flow-limiting (case 2) and unstable (case 3); and (b) the experimental results of the maximal flow rates passing through the flow-regulating reservoirs with different diameters plotted along with the theoretical simulations, in which inserted snapshots illustrate the deformation of gas-liquid interface at different states.

Flow-controlled switching

Furthermore, utilizing the deformable interface with flow-limiting characteristics described above, a 3D flow-controlled switch is devised between two patterned substrates. As shown in Fig. 3, the fluidic switch can be selectively activated in one of the compliant reservoirs where a miniature capillary bridge forms between two surfaces. In principle, when fluid passes through two different capacitive elements connected by serial resistive channels, the interfacial deformation in each reservoir depends on the inflow rate and geometric dimensions of both capacitive and resistive units. For the sake of simplicity, we utilize the binary code to describe the switch performance. Under low inflow rates (< Q_{max} of Reservoir 1), majority of fluid moves towards the larger reservoir (Reservoir 0) at the end, of which the interface expands vertically in a faster pace under the same pressure head according to Laplace equation, and thus, connects to the flow path on the upper surface, *i.e.*, the '0' path is activated/ON (Fig. 3-a). While at high influxes (> Q_{max} of Reservoir 1), the smaller reservoir (Reservoir 1) accumulates most of fluid first and deforms the interface at a higher speed due to the flow-limiting function, and thereby, the flow switch to the '1' path on the top layer (Fig. 3-b). As can be seen, by including contacting reservoirs from the top surface, the capillary bridge can be switched ON controllably (see Movie 2 in ESI). Fig. 3-c and 3-d show the inflow waveforms to activate individual switches along with the corresponding height variations of the deformed interfaces in both reservoirs from the simulated results. Fig. 4 illustrates the equivalent circuit model for the flow-controlled switch, which has been used in the simulation. In particular, the ground of the fluidic network represents the ambient pressure, while in the outflow path, the fluid is directed toward the collective reservoir with centimeter sizes, of which the pressure inside is approximated to the ambience. Moreover, Zener diodes with an activation threshold closely resemble the characteristics of fluidic activation through one-way formation of the capillary bridges, of which the threshold pressure (equivalent to the break-through voltage) is determined by both the dimensions of the capacitive reservoirs and the height of the spacers. It is worth noting that once the liquid bridge forms, the flow rate can be reduced to a lower steady-state level for subsequent fluidic operations. The primary shortcoming of the lumped-element model is that it cannot precisely describe the reverse fluidic switching process due to the hysteretic operation of the capillary bridge diodes. In brief, the flow-controlled switch is capable of directing flow into two separate channels by comparing with a threshold flow rate (Q_{max} of Reservoir 1), analogous to the function of a comparator in an electronic circuit.

Analog-to-digital stereo-flow activations

Three-dimensional surface microfluidic networks can be devised by simply connecting two independent planar fluidic circuits through miniature capillary bridges. Fig. 5 shows a prototype of a stereo microfluidic chip incorporating parallel streams flowing in three-dimensional helical patterns. Surface flow begins in the

 This journal is © The Royal Society of Chemistry 2010

View Online

Downloaded by Library of Chinese Academy of Sciences on 26 November 2010
Published on 09 November 2010 on http://pubs.rsc.org | doi:10.1039/C0LC00173B

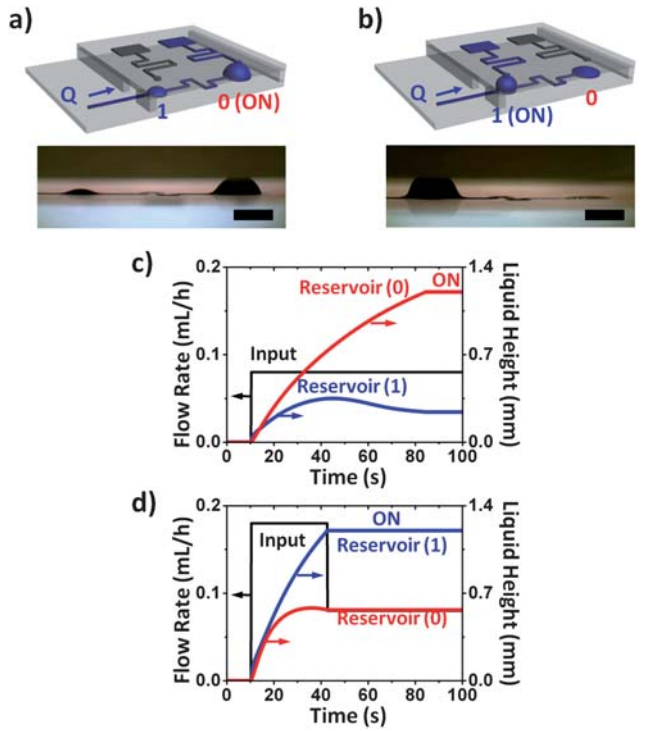

Fig. 3 (a,b) Schematic illustrations (top) along with side views (bottom) of the flow rate-controlled switching; (c,d) the inflow waveforms to activate individual switches with the corresponding height variations of the deformed interfaces in both reservoirs (scale bars: 1mm).

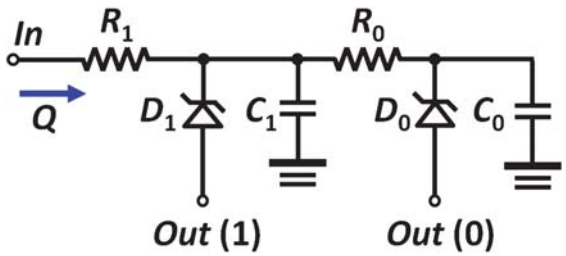

Fig. 4 The equivalent circuit model for the flow-controlled switch, where Zener diodes with an activation threshold represent one-way formation of the capillary bridges.

hydrophilic channel on the bottom substrate, and accumulates and deforms the gas-liquid interface in the first reservoir. Once it reaches the top surface separated by a spacer, a capillary bridge forms between two opposite wettability-defined reservoirs on the top and bottom substrates. While the geometry of microchannels confines the vertical expansion of the interfaces, leaving the fluidic contacts only through the capillary bridge formed between two capacitive elements. The streaming and connecting patterns run repetitively between the top and bottom surfaces and eventually evolves into three-dimensional flow without intercepting with each other, as shown in Fig. 5. In brief, the surface flow travels in plane as directed by the open microfluidic network, while forming transverse fluidic path through the established capillary bridges (as interfacial capacitive expansion).

Integrating the flow-controlled switching function with 3D surface flows, digital fluidic networks can be realized with multichannel analog-to-digital flow activation, analogous to an analog-to-digital converter in the circuits. As shown in Fig. 6, the flow-controlled switches have been incorporated in a multi-stage configuration between the top and bottom substrates. According to the aforementioned flow switching model, the activation threshold (Q_{max}) of the device sets the margin to direct flow into the designated binary branch. In this configuration, binary outputs from one flow-controlled switch feed into two switches in the next stage, while each switch keeps a distinct activation threshold for further flow-controlled splitting. By doubling flow switches in each serial add-on stage, we could potentially expand to 2^N-level analog-to-digital flow activation (where N is the number of stages). Therefore, the flow rate-directed multiplexing can be further refined and function as an analog-to-digital flow activation device. Moreover, by withdrawing the liquid from previous actuation, the connected fluidic switch through capillary bridge can be turned off, while new connections/switch operations can be performed subsequently according to the next activation flow waveform. As shown in Fig. 7, four (2^2) channel switching/activation with individual addressability has been implemented by including two-stage flow switching devices with three-level threshold settings (Q^0_{max}, Q_{max}, and Q^1_{max}). For instance, the activation flow pulse between Q^0_{max} and Q_{max}

Fig. 5 A three-dimensional surface microfluidic chip incorporating parallel streams flowing in three-dimensional spiral patterns (Scale bar: 2mm).

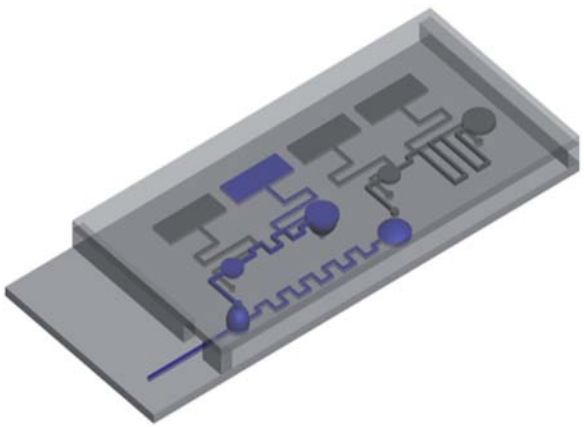

Fig. 6 Schematic drawing of the two-stage analog-to-digital flow activation.

View Online

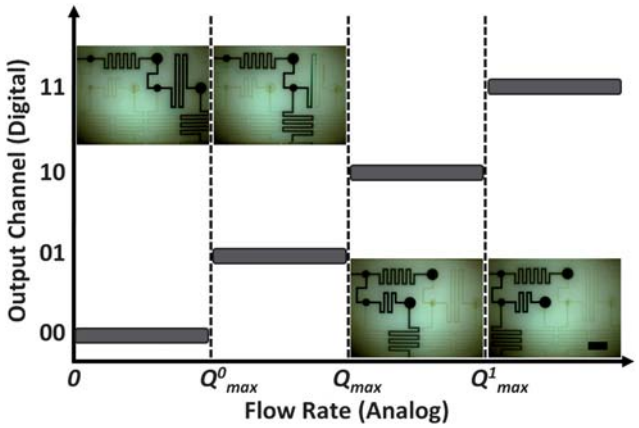

Fig. 7 Four-channel analog-to-digital flow activation, along with the snapshots of the function device with individual addressability (scale bar: 2mm).

directs the flow towards '01' path, whereas flow rates between Q_{max} and Q^1_{max} result in passing through '10' path (see Movie 3 in ESI). Figure S1 provides the extended circuit model to simulate the multi-level flow activation. Overall, the analog-to-digital flow-switching network has been first demonstrated in the three-dimensional surface microfluidics by only tuning the inflow pulse and the multi-stage expandability has illustrated its potential use for the large-scale integration of digital fluidics. Furthermore, complex digital microfluidic operations are currently under investigation.

Conclusions

By introducing an elastic gas-liquid interface, surface microfluidic networks offer novel spatiotemporal fluidic manipulations on the planar surfaces. Using a one-step microfabrication of the superhydrophobic nanocomposite material, ultrahigh wettability contrast on a hydrophilic substrate can be established, which permits surface flow on a single planar substrate. Detailed theoretical analysis, using the lumped-element model, incorporates both basic capacitive (circular micro-reservoir) and resistive (straight microchannel) elements in the open fluidic platform. Further manipulations on the lateral deformable and time-dependent interfaces lead to novel surface microfluidic functions, *i.e.*, microflow regulation and flow-controlled switching. The microflow regulator provides the functions of overflow protection, while the flow-controlled switch allows individual activation of the specific fluidic path under the corresponding flow rate. Furthermore, three-dimensional surface microfluidic networks have been successfully devised by connecting two independent planar fluidic circuits through miniature capillary bridges. The flow-controlled switching concept has been extended to multi-level operations in the stereo-fluidic network, performing as an analog-to-digital converter in electronic circuits. In summary, surface microfluidics, governed by elastic frictionless gas-liquid and inflexible resistive solid-liquid interfaces, opens new possibilities to maneuver microflow in three-dimensional and time-dependent fashions, which can be further explored in digital and biomedical microfluidic applications.

Published on 09 November 2010 on http://pubs.rsc.org | doi:10.1039/C0LC00173B
Downloaded by Library of Chinese Academy of Sciences on 26 November 2010

Acknowledgements

This work is in part supported by the National Science Foundation (CAREER ECCS-0846502 and CMMI-0944353). LH acknowledges the fellowship support from China Scholarship Council (CSC).

References

1 P. Gravesen, J. Branebjerg and O. S. Jensen, *J. Micromech. Microeng.*, 1993, **3**, 15.
2 D. J. Beebe, G. A. Mensing and G. M. Walker, *Annu. Rev. Biomed. Eng.*, 2002, **4**, 26.
3 G. M. Whitesides, *Nature*, 2006, **442**, 6.
4 M. J. Swickrath, S. D. Burns and G. E. Wnek, *Sens. Actuators, B*, 2009, **140**, 7.
5 K. Kim, D. S. Park, H. M. Lu, W. Che, K. Kim, J.-B. Lee and C. H. Ahn, *J. Micromech. Microeng.*, 2004, **14**, 7.
6 M. Abdelgawad, M. W. L. Watson and A. R. Wheeler, *Lab Chip*, 2009, **9**, 6.
7 G. M. Walker and D. J. Beebe, *Lab Chip*, 2002, **2**, 4.
8 M. Tokeshi, T. Minagawa, K. Uchiyama, A. Hibara, K. Sato, H. Hisamoto and T. Kitamori, *Anal. Chem.*, 2002, **74**, 7.
9 T. Maruyama, J.-i. Uchida, T. Ohkawa, T. Futami, K. Katayama, K.-i. Nishizawa, K.-i. Sotowa, F. Kubota, N. Kamiya and M. Goto, *Lab Chip*, 2003, **3**, 5.
10 B. D. Piorek, S. J. Lee, J. G. Santiago, M. Moskovits, S. Banerjee and C. D. Meinhart, *Proc. Natl. Acad. Sci. U. S. A.*, 2007, **104**, 4.
11 L. Hong and T. Pan, in *IEEE MEMS*, Hongkong, 2010.
12 L. Hong and T. Pan, *JMEMS*, 2010.
13 B. Zhao, J. S. Moore and D. J. Beebe, *Anal. Chem.*, 2002, **74**, 10.
14 B. Zhao, N. O. L. Viernes, J. S. Moore and D. J. Beebe, *J. Am. Chem. Soc.*, 2002, **124**, 2.
15 S. Bouaidat, O. Hansen, H. Bruus, C. Berendsen, N. K. Bau-Madsen, P. Thomsen, A. Wolff and J. Jonsmann, *Lab Chip*, 2005, **5**, 10.
16 J. West, A. Michels, S. Kittel, P. Jacob and J. Franzke, *Lab Chip*, 2007, **7**, 3.
17 M. Watanabe, *Lab Chip*, 2009, **9**, 4.
18 A. Aota, A. Hibara and T. Kitamori, *Anal. Chem.*, 2007, **79**, 6.
19 B. Zhao, J. S. Moore and D. J. Beebe, *Science*, 2001, **291**, 4.
20 H. Gau, S. Herminghaus, P. Lenz and R. Lipowsky, *Science*, 1999, **283**, 4.
21 D. Juncker, H. Schmid, U. Drechsler, H. Wolf, M. wolf, B. Michel, N. d. Rooij and E. Delamarche, *Anal. Chem.*, 2002, **74**, 6.
22 M. Watanabe, *Microfluid. Nanofluid.*, 2010, **8**, 6.
23 M. J. Swickrath, S. Shenoy, J.A.M. Jr., J. Belcher, R. Kovar and G. E. Wnek, *Microfluid. Nanofluid.*, 2008, **4**, 11.
24 J. W. Suk and J.-H. Cho, *J. Micromech. Microeng.*, 2007, **17**, 6.
25 S. S. Sridharamurthy and H. Jiang, *IEEE Sens. J.*, 2007, **7**, 2.
26 P. Lam, K. J. Wynne and G. E. Wnek, *Langmuir*, 2002, **18**, 4.
27 J. S. H. Lee, I. Barbulovic-Nad, Z. Wu, X. Xuan and D. Li, *J. Appl. Phys.*, 2006, **99**, 8.
28 E. Besson, A.-M. Gui, J. Sudor, H. Korri-Youssoufi, N. Jaffrezic and J. Tardy, *Langmuir*, 2006, **22**, 7.
29 A. M. Skelley and J. Voldman, *Lab Chip*, 2008, **8**, 1733–1737.
30 M. Zimmermann, P. Hunziker and E. Delamarche, *Microfluid. Nanofluid.*, 2008, **5**, 395–402.
31 P. F. Man, C. H. Mastrangelo, M. A. Burns and D. T. Burke, *IEEE*, 1998, 6.
32 A. Gliere and C. Delattre, *Sens. Actuators, A*, 2006, **130–131**, 8.
33 C. N. Baroud, J. P. Delville, F. Gallaire and R. Wunenburger, *Phys. Rev. E: Stat., Nonlinear, Soft Matter Phys.*, 2007, **75**.
34 H. Cho, H.-Y. Kim, J. Y. Kang and T. S. Kim, in *Technical Proceedings of the 2004 Nanotechnology Conference and Trade Show*, 2004.
35 C. Bowick, C. Ajluni and J. Blyler, *RF Circuit Design*, Newnes, 2007.
36 J. Melin, W. van der Wijngaart and G. Stemme, *Lab Chip*, 2005, **5**, 682–686.
37 B. Yang and Q. Lin, *Microelectromechanical Systems, Journal of*, 2007, **16**, 9.
38 W. Xu, L. L. Wu, Y. Zhang, H. Xue, G.-P. Li and M. Bachman, *Sens. Actuators, B*, 2010, **142**, 7.

 This journal is © The Royal Society of Chemistry 2010